Journal of Applied Fluid Mechanics, Vol. 17, No. 7, pp. 1470-1484, 2024.
Available online at www.jafmonline.net, ISSN 1735-3572, EISSN 1735-3645.
https://doi.org/10.47176/jafm.17.7.2421

Stall Inception Control by Setting Groove Based on Its Formation Mechanism in Centrifugal Impeller

X. D. Liu[1], X. B. Huang[1], Y. J. Li[2], Z. Q. Liu[2,3,4†] and W. Yang[2]

[1] *College of Electrical, Energy and Power Engineering, Yangzhou University, Yangzhou 225009, China*
[2] *College of Water Resources and Civil Engineering, China Agricultural University, Beijing 100083, China*
[3] *School of Water Conservancy and Civil Engineering, Northeast Agricultural University, Harbin 150030, China*
[4] *Beijing Engineering Research Center of Safety and Energy Saving Technology for Water Supply Network System, China Agricultural University, Beijing 100083, China*

†Corresponding Author Email: lzq@cau.edu.cn

ABSTRACT

Stall, a complex flow phenomenon in centrifugal pump, plays a crucial role in pump safety and stability under part-load conditions. In this paper, a verified numerical simulation method is employed to analyze the three-dimensional flow field under the stall inception conditions. The results reveal the initial stall vortex occurs near the Q=0.7Qd condition in the prototype impeller. Based on stall formation mechanism, the high-velocity fluid near the blade pressure side is sucked into suction side of next impeller channel by setting a groove near the blade leading edge. This jet flow can prevent the narrow vortices near the impeller shroud from moving towards the blade suction side, thereby suppressing the formation of stall vortex. By comparing the effects of different groove locations, directions, and sizes on stall vortex control, the optimal groove width is determined to be approximately 1mm. Compared with the prototype impeller, the grooved impeller can completely eliminate the stall vortex and significantly reduce pressure pulsation under part-load conditions. Moreover, the head of grooved impeller is increased by nearly 15% under Q=0.6Qd condition, and the potential suppression mechanism is also explained. Based on the stall formation mechanism, this paper puts forward an effective stall control method, which delays the stall inception significantly.

Article History

Received November 5, 2023
Revised January 8, 2024
Accepted February 5, 2024
Available online April 30, 2024

Keywords:

Numerical simulation
impeller
groove
narrow vortex
stall control

1. INTRODUCTION

Stall is a complex flow phenomenon that occurs in centrifugal pump under part-load conditions. Under stall conditions, centrifugal pumps often experience the phenomena of energy conversion instability, intensified of vibration and noise, and even blade fatigue failure (Tanaka, 2010; Zhao et al., 2018; Lu et al., 2020). The emergence of unevenly distributed stall vortex in the impeller also leads to radial force (Jia et al., 2019). These phenomena usually destroy impeller structure and result in significant fluctuation in pump's head and efficiency. Therefore, researchers have adopted various methods to control stall (Guo & Maruta 2005; Gölcü & Sekmen 2006). An effective method of suppressing stall is to employ specific techniques to suppress occurrence of the stall vortex under part-load conditions, thereby broadening the pump's stable operation range.

Based on previous research, there are three main methods to control unsteady flow phenomenon in centrifugal pumps. The first method is to suppress the generation of separation vortex at the inlet of impeller channel. Some studies have suggested that as the flow rate decreases, the incidence angle at the channel inlet increased, resulting in the formation of separation vortices. (Korkmaz & Kurbanoğlu. 2017, Gölcü & Pancar 2005). Based on these conclusions, Luo et al. (2020) explored the effect of different leading-edge shapes on the distribution of stall vortices in the impeller channel using numerical simulation method. The results showed that there was a close relationship between the shape of blade leading edge and the distribution of stall vortices in impeller channels. Kyparissis & Margaris, (2012) also designed three different blade leading-edge shapes and proposed that reasonable leading-edge shape could reduce cavitation and improve the pump performance. Korkmaz & Kurbanoğlu (2017) investigated the effects of the incidence angle, number of blades and splitter blades on pump performance. Song et al. (2015) investigated the influence of blade profile

shapes on cavitation behavior in centrifugal pump. The results show a small change in blade incidence angle resulted in a significant separation of the cavitation region near the blade suction side. Sato & Takamatsu (1993) also focused on the influence of the channel incidence angle on the pump performance. In addition to blade leading-edge shape, some scholars have also investigated the influence of the blade trailing-edge on the internal and external characteristics of the pump. Cui et al. (2020) also investigated the impact of various blade trailing-edge geometries of the pump under part-load conditions. The findings indicate that an appropriate cutting angle could effectively reduce the intensity of wake vortex. However, engineering experience suggests that the smaller the change in impeller geometry, the smaller impact on the centrifugal pump performance. The results show that only when the modification of impeller geometry is less than 0.1% of the impeller diameter, its impact on pump's head and efficiency can be ignored (Cui et al., 2020). The first method primarily focuses on the influence of blade leading-edge or trailing-edge shape on the pump's external characteristics. However, the relationship between blade geometry and stall formation mechanism is not yet clear.

The second method typically employs splitter blades to control the stall vortex (Yuan & Yuan 2017; Davood & Shirani 2018; Adu et al., 2021). The primary objective of this approach is not to control the emergence of the stall vortex at the source, but rather to suppress its further growth. Kergourlay et al. (2007) investigated the impact of arranging splitter blades in the impeller, finding that this method can effectively reduce pressure pulsation within the impeller. Onoue et al. (2016) examined the influence of splitter blade near the blade suction side on the flow field, observing that splitter blades near the blade suction side can effectively enhance the pump performance. Yuan & Yuan (2017) discovered adding short blades could significantly improve impeller head and efficiency, and result in a more uniform distribution of turbulent kinetic energy within the impeller. Shojaeefard et al. (2012) investigated the influence of impeller geometry on the pump performance. The results show that when the impeller outlet angle was 30 degrees and the channel width was 21mm, energy loss could be significantly reduced and the vortex structure could be effectively restrained within the impeller. However, for different sizes of centrifugal pumps, these parameters should be adjusted appropriately to achieve optimal results. After adding splitter blades, the increasing stall vortex within the impeller can be restrained, and the radial flow field becomes more uniform (Chiang & Fleeter, 1994; Shigemitsu et al., 2013). Although the splitter blades can control the flow in the impeller, this method obviously alters the impeller geometric structure, which must result in significant changes to the pump external characteristics.

The third method involves improving centrifugal pump performance by incorporating grooves. This flow control technology utilizes the pressure difference between the blade pressure side and the suction side to channel fluid near the high-pressure side through the grooves, thereby enhancing the velocity near the blade suction side. Initially, this grooving method was primarily employed in compressors (Zhu et al., 2006; Zhou et al., 2017). In reality, its application in centrifugal pump impellers aimed to control cavitation. Cui et al. (2019) utilized the active jet method to suppress cavitation, demonstrating that that a 6% jet flow rate can achieve better cavitation control effect. Wu et al. (2021) placed the groove at a position 1/4 away from the blade inlet, observing a decrease in head and efficiency at the design condition. Khoeini & Shirani (2019) concluded that the guide vane height had an important impact on the performance of centrifugal pump, but the groove significantly reduced the pump head and efficiency. Du et al. (2011) designed grooves in a high-load turbine. It shows that at low Reynolds number, it could effectively compress flow separation and reduce energy loss, but the position and shape of grooves required further study. Considering the existing research, it indicates that the groove control technology is widely used in centrifugal compressor or for suppressing cavitation, while its effectiveness in controlling stall vortex in centrifugal pump is relatively limited. The formation mechanism of stall in the impeller remains unclear, preventing further comparison and analysis on the groove location, direction and size.

Therefore, based on the formation mechanism of stall vortex, this paper conducts a comprehensive analysis of the stall control mechanism of groove method. The results show that a reasonable grooved impeller can not only ensure that the pump's head and efficiency remain unchanged at design flow and high flow rate conditions, but also significantly improve the pump head at part-load conditions. The groove suppresses the appearance of stall vortex and reduces pressure pulsation in the impeller effectively.

2. NUMERICAL SIMULATION

2.1 Impeller Model

A low specific-speed centrifugal impeller (n_s=80), with main model parameters referenced from the study by Pedersen et al. (2003). The impeller speed is S=725r/min, and the design flow rate Qd=3.06kg/s. The entire calculation domain is divided into three parts: the inlet, impeller and outlet section. The grooved impeller involves designing grooves at appropriate position on the impeller blades. The fluid domains of prototype impeller and grooved impeller are shown in the Fig.1. The d is groove width, and ensuring the grid quality in the groove area is crucial for simulation accuracy.

2.2 Model Grid and Validation

To ensure the grid accuracy in the groove area, a structured grid based on CFX 18.2 ICEM was used to discrete the grooved and prototype impellers. The inlet and outlet sections of the two types of impeller were consistent. For both types of impellers, the y^+ values on the wall was less than 1.5. Different grids scales were used to perform the grid independence test 2.1×10^6,2.6×10^6,3.1×10^6,3.6×10^6, 4×10^6 nodes. When the number of grids reaches 3.1×10^6, the relative differences

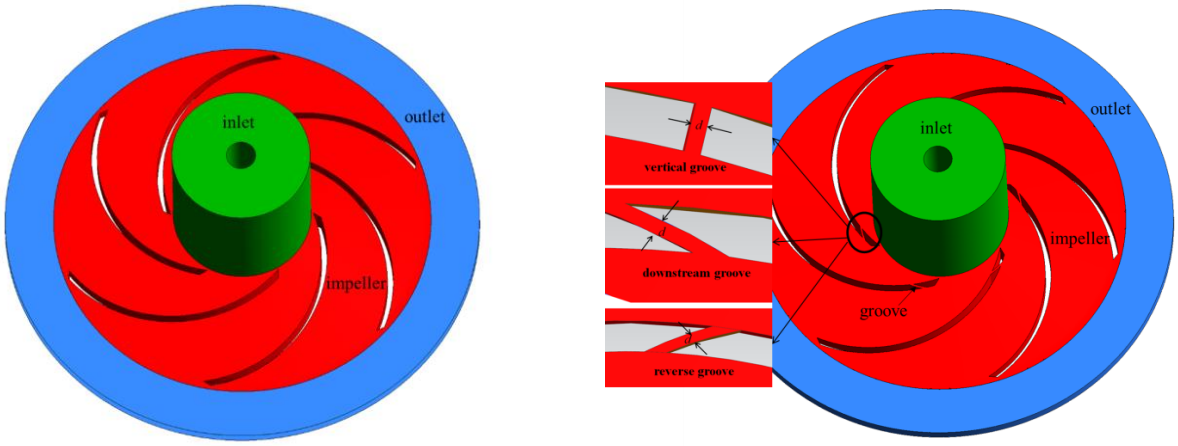

(a) the fluid domain of prototype impeller (b) the fluid domain of grooved impeller

Fig. 1 Fluid domains of prototype and grooved impellers

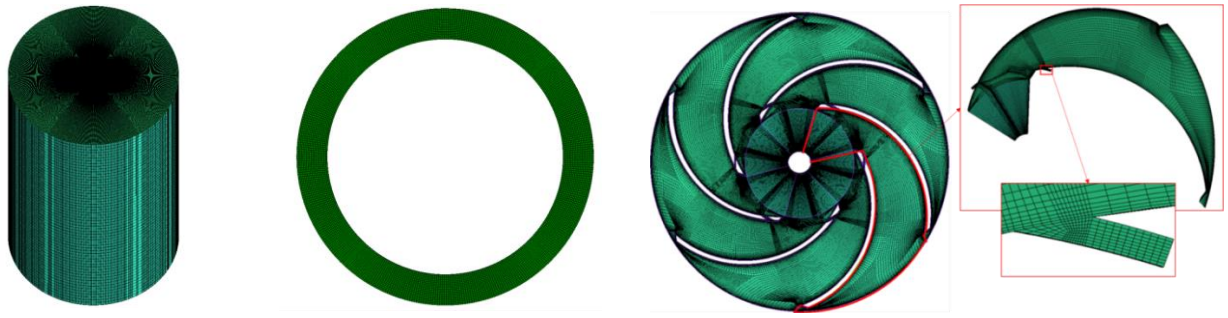

(a) the inlet section grid (b) the outlet section grid (c) the grooved impeller grid

Fig. 2 Grid of whole grooved impeller fluid domain

of impeller head was lower than 1.5%. The total number of grids for two impeller forms was almost the same. Finally, a grid scale of 3.1million was chosen. The grid form of the grooved impeller is shown in the Fig.2.

2.3 Turbulence Models and Boundary Conditions

The governing equations of the fluid flow include the continuity equation and the momentum equation as shown in Eq. (1) and (2).

$$\frac{\partial u_i}{\partial x_i} = 0 \tag{1}$$

$$\frac{\partial(\rho u_i)}{\partial t} + \frac{\partial}{\partial x_j}(\rho u_i u_j) = -\frac{\partial p}{\partial x_j} + \frac{\partial}{\partial x_j}[\mu(\frac{\partial u_i}{\partial x_j} + \frac{\partial u_j}{\partial x_i})] \tag{2}$$

Where u_i is the time averaged velocity component, p is the time averaged pressure and μ_t is the dynamic viscosity. x_i and x_j are the components of the Cartesian coordinate system; u_i and u_j are the velocity components of the fluid.

The model impeller was numerically using commercial software ANSYS CFX 18.2. A mass flow was set as the inlet boundary condition, and a pressure with relative pressure 1atm was set as outlet boundary condition. The impeller domain and outlet domain were connected using "Transient Rotor-stator" to realize the data transfer between the upstream and the downstream. Other parts were set as slip wall as wall boundary. The time step was set to 2.3×10^{-4} s (equivalent to a pitch of 2°), and the convergence criterion was 1×10^{-5}. In order to accelerate the convergence of the simulation, the SST *k-w* model was used to obtain steady-state convergence result.

The specific expression of the SST *k-w* model has been presented in detail in (Ye et al., 2020) The transient calculation using the SAS-SST model has been elaborated in detail in (Jadidi et al., 2018). The unsteady results were calculated for 10 impeller cycles, and the last 5 cycles were used for time-average result. The accurate prediction of the SST-SAS turbulence model for the flow field in the impeller is crucial for revealing the mechanism suppression of stall by grooves. The prediction accuracy of this turbulence model has been fully validated in previous studies, mainly including the distribution characteristics of stall vortices in the impeller channel under different conditions and the quantitative velocity comparison on different sample lines under typical conditions (Liu et al. 2023). The average relative velocity error can be controlled within 10%. A comparison of time-averaged results from experimental results and numerical simulation under Q=0.4Qd is shown in the Fig.3.

3. NUMERICAL RESULTS

Next, a numerical simulation method was employed to comparatively analyze the flow field characteristics in both the prototype impeller and the grooved impellers. Meanwhile, the flow field characteristics in the impeller

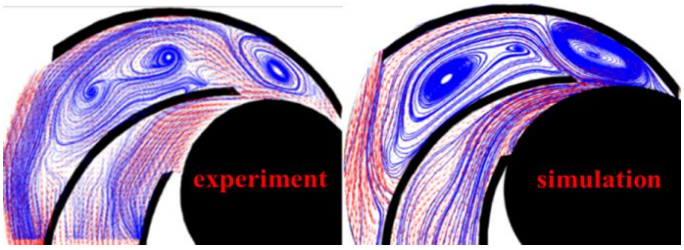

Fig. 3 Comparison of experimental and numerical simulation results of flow field in impeller under Q=0.4Qd

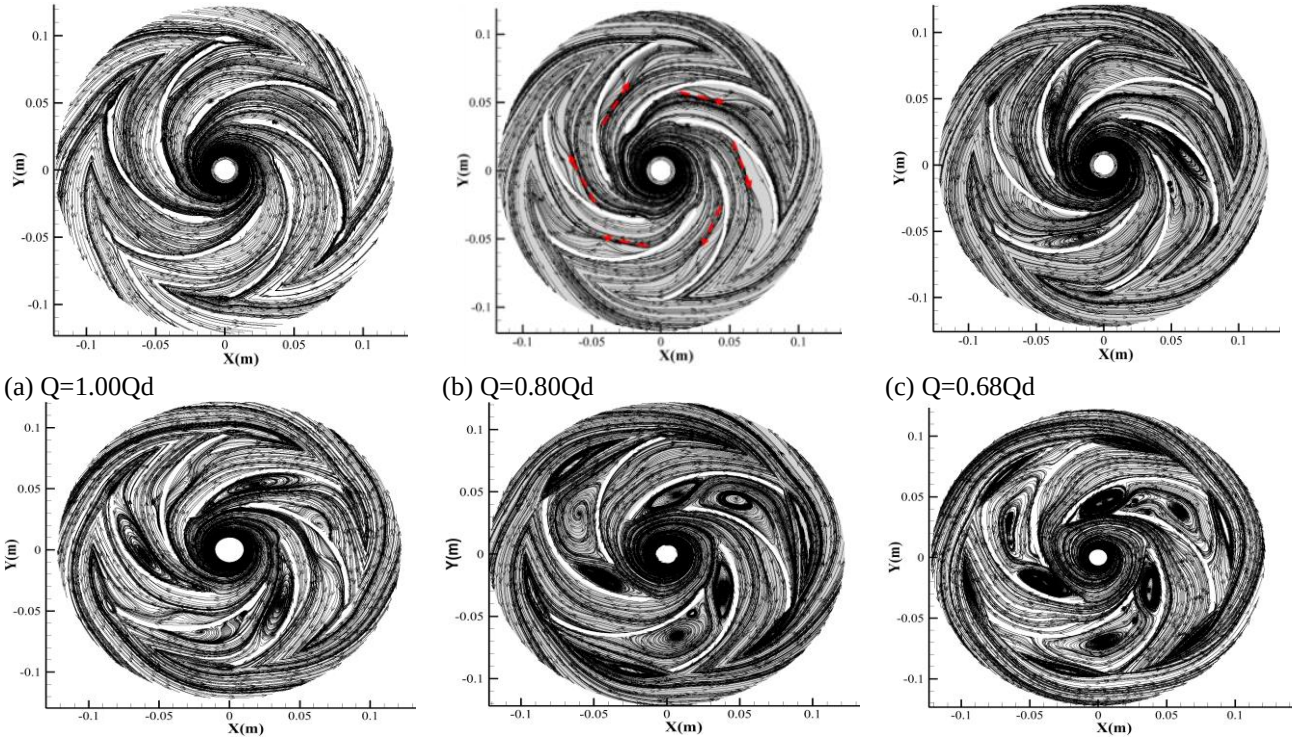

(a) Q=1.00Qd (b) Q=0.80Qd (c) Q=0.68Qd

(d) Q=0.65Qd (e) Q=0.50Qd (f) Q=0.40Qd

Fig. 4 Results of the time-averaged flow field inside the impeller under several different flow rate conditions.

with different groove parameters were compared to determine the optimal groove configuration.

3.1 Characteristics of Prototype Impeller at Different Flow Rate Conditions

Figure 4 presents the two-dimensional relative velocity field within the impeller under various flow rate conditions. The two-dimensional plane is located at half the height of the impeller outlet. When the impeller operates under Q=1.0Qd condition, as shown in Fig. 4(a), the streamline flows tightly along blade suction side. With the decrease in flow rate, as indicated by the red arrow in Fig. 4(b), the flow begins to deviate from the blade suction side. Subsequently, a vortex structure emerges near the blade suction side, as shown in Fig. 4(c). As the flow rate continues to decrease, the alternating stall phenomenon becomes more intense, as seen in Figs. 4(d)-(f). Fig.4 primarily demonstrates the flow field characteristics within the impeller under several typical flow rate conditions. The more detailed evolution process of stall vortex within the impeller has been described in the experiment conducted by (Liu et al., 2022).

Figure 5 presents the flow field characteristics in the impeller using two methods. The first approach is to showcase the characteristics through a two-dimensional plane, and the second approach utilizes uniformly velocity starting points on the circumferential section of the inlet arc of the impeller channel 1, displaying the three-dimensional flow field characteristics within the impeller. It presents that a narrow vortex strip exists near impeller shroud. Under Q=1.0Qd condition, as shown in Fig. 5(a), the vortex strip is primarily located in the middle of the impeller shroud. With the decrease of flow rate, as shown in Fig. 5 (b) and (c), the vortex strip gradually extends towards the blade suction side, resulting in flow separation nearby. The flow separation further evolves into a stall vortex in Fig. 5 (d). Therefore, the transfer of twisted vortex strip near the impeller shroud to the blade suction side is the direct reason for the emergence of stall vortex with the decrease in flow rate.

Based on the mechanism of stall formation, it indicates that if the vortex strip near the impeller shroud can be effectively restrained from extending to the blade suction side, the occurrence of the stall vortex can be effectively suppressed. Therefore, the jet flow method can be utilized to suppress the stall vortex within the impeller.

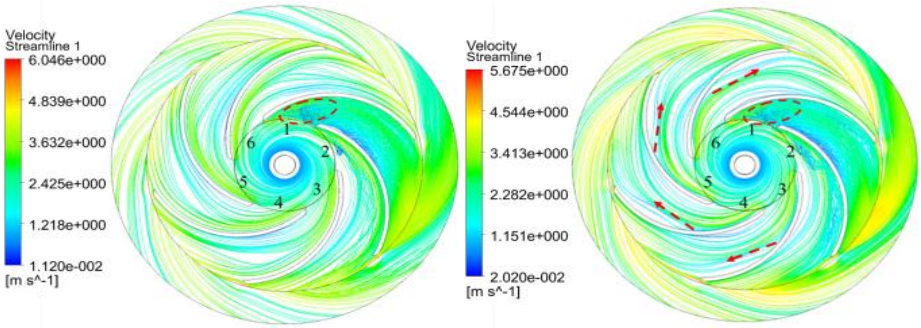

(a) Q=1.0Qd (b) Q=0.9Qd

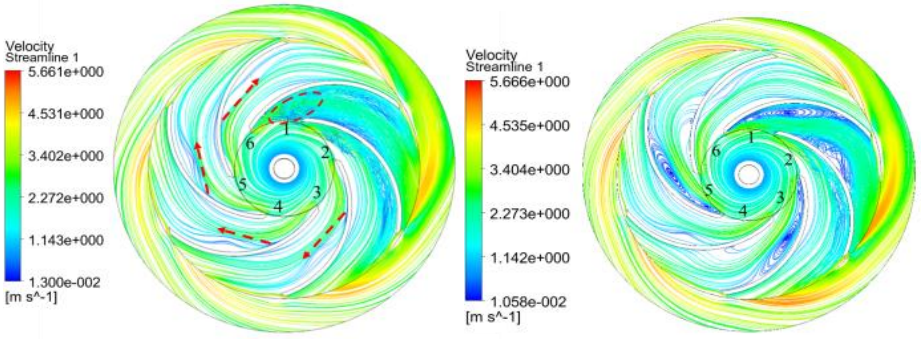

(c) Q=0.8Qd (d) Q=0.68Qd

Fig. 5 Two-dimensional and three-dimensional flow field characteristics in impeller under different flow rate conditions

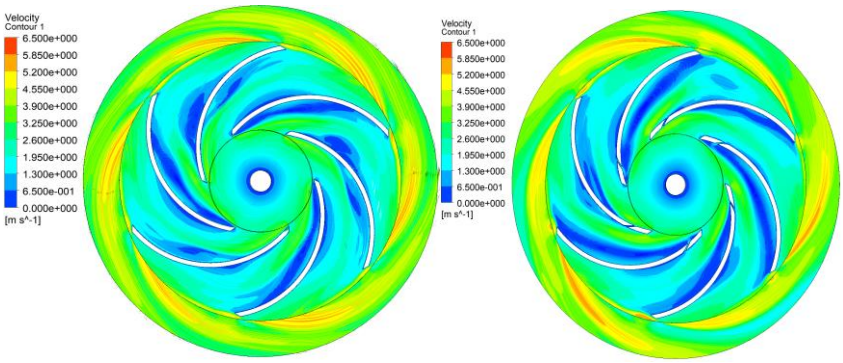

(a) prototype impeller (b) reverse groove

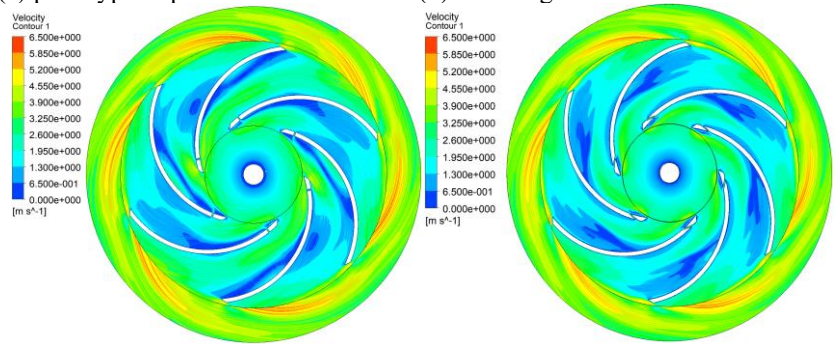

(c) perpendicular groove (d)downstream groove

Fig. 6 Control effect of different groove directions on stall vortex under Q=0.68Qd condition

3.2 Effect of Different Groove Directions on Stall Vortex

A prototype impeller was used to compare with the impeller with different groove directions to determine the optimal model. Based on the results in Fig.5, the inhibitory effect of different groove directions on stall vortex at the Q=0.68Qd condition was further compared. The Fig.6 shows the comparison between the prototype impeller and several different grooved impellers. When the groove direction is set as shown in Fig. 6(b), a larger

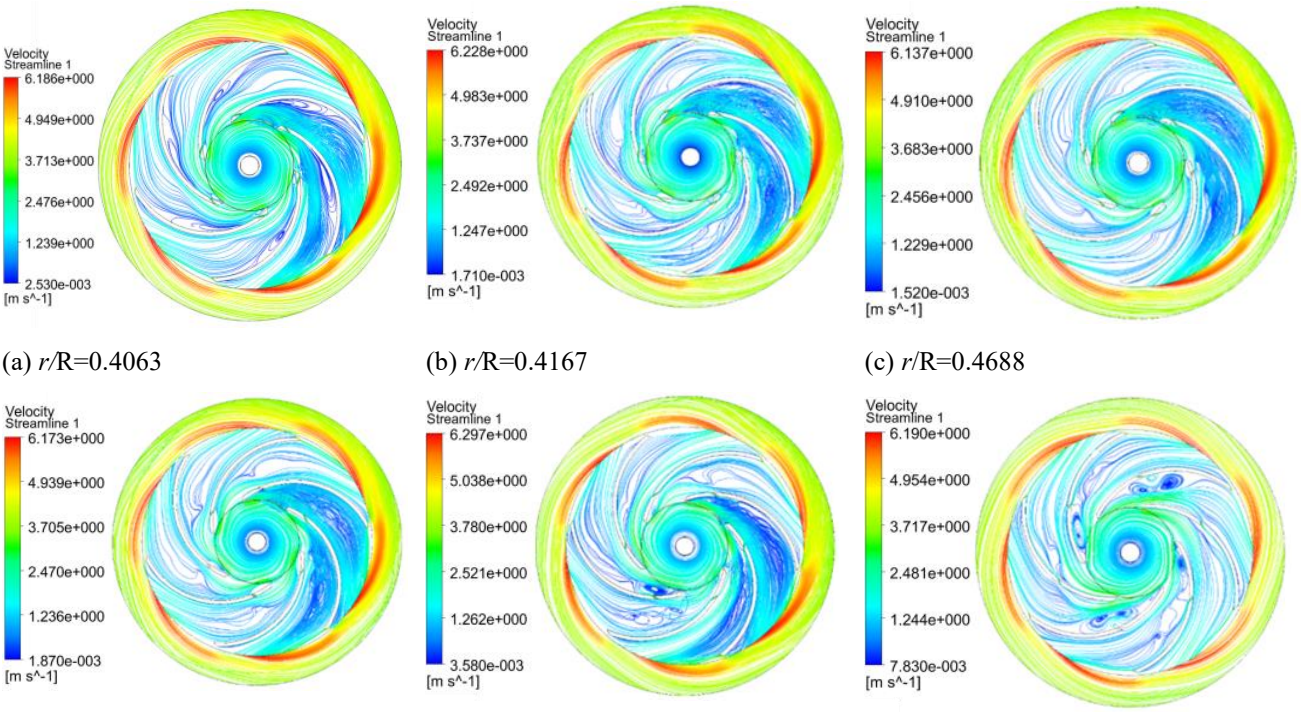

(a) *r*/R=0.4063 (b) *r*/R=0.4167 (c) *r*/R=0.4688

(d) *r*/R=0.5000 (e) *r*/R=0.5478 (f) *r*/R=0.6093

Fig. 7 Control effect of different groove positions on stall vortex under Q=0.5Qd condition

low-velocity area appeared near the blade suction side. When the groove direction is perpendicular to the blade surface in Fig. 6(c), large area of low-velocity appeared near both the blade suction and pressure sides, but it still can't restrain the appearance of stall vortex. However, it suppressed the expansion of the low-velocity area in Fig. 6 (d). The vortex structure near the blade suction side disappears obviously, and the flow in the impeller channel is smoother. By designing different groove directions, the results show that taking the impeller center as the center, the overlapping area of the circular ring and the blade is determined as the optimal groove form as shown in Fig. 6(d). After determining the groove direction, the inhibition effect of the groove position on stall vortex was further analyzed.

3.3 Effect of Different Groove Positions on Stall Vortex

In addition to the proper groove direction, the groove position is also a crucial factor affecting stall control effect. Next, the impact of different groove positions on stall vortex was further explored. Through calculations, it was found that when the flow rate was greater than Q=0.5Qd, the flow field characteristics were basically the same for impellers with different groove positions. Therefore, the control effect of different groove positions on stall vortex was evaluated at Q=0.5Qd condition, as shown in Fig.7. Here, *r* represents radial position of the groove, and R represents the radius of the impeller. The two-dimensional flow field of the impeller prototype at Q=0.5Qd condition was drawn in Fig. 4 (e). When the relative position of the groove was close to the blade leading edge, as shown in Fig. 7 (a), the jet flow eliminated the separation vortex at the channel inlet significantly. However, the effect of restraining the vortex near impeller shroud from moving to the blade suction side was significantly weakened. It was observed that an obvious vortex structure appeared near the middle position of the blade suction side in each impeller channel, as shown in Fig. 7(a). For the groove relative position ranging from *r/R*=0.4167 to *r/R*=0.50, the stall vortex in the impeller channel disappeared completely as shown in Fig. 7 (b) to Fig. 7 (d). This is because the jet flow could not only block the expansion of the separation vortex at the channel inlet, but also effectively suppressed the further intensification of the flow separation near the blade suction side. Therefore, under this condition, the separation vortex at the channel inlet and the separation vortex in the middle position near the blade suction side cannot merge. This indicates the jet flow could suppress the stall occurrence of stall at the source. However, when the relative position of the groove was greater than *r/R*=0.5478, as shown in Fig. 7 (e), the jet flow cannot prevent the expansion of the vortex structure at the channel inlet. Therefore, the effect of the jet flow was weakened significantly, as shown in Fig.7 (e) and Fig. 7 (f).

3.4 Effect of Different Groove Sizes on Stall Control

Groove width is another crucial parameter that influences the stall control effect. Building upon the results obtained in Section 3.3, the relative position of the groove was fixed at *r*/R=0.4688, and the influence of various groove widths on the stall vortex was further investigated. The flow rate conditions of Q=0.5Qd and Q=0.4Qd are selected as the targets. Subsequently, the jet flow effects for different groove widths, namely 0.25mm, 0.5mm, 1mm, 2mm, and 3mm, were compared

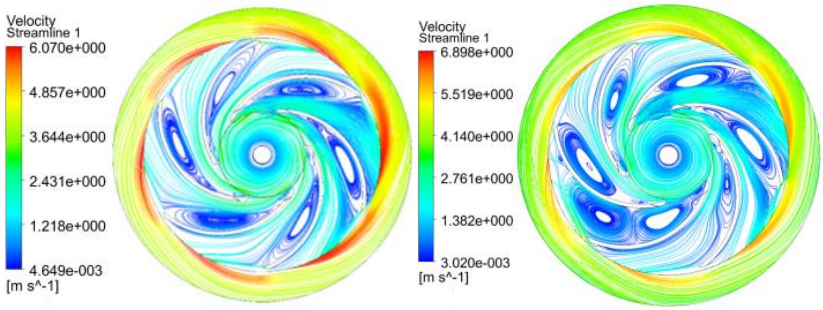

(a) Q=0.5Qd (b) Q=0.4Qd

Fig. 8 Control effect of groove width 0.25mm on stall vortex at Q=0.5Qd and Q=0.4Qd conditions

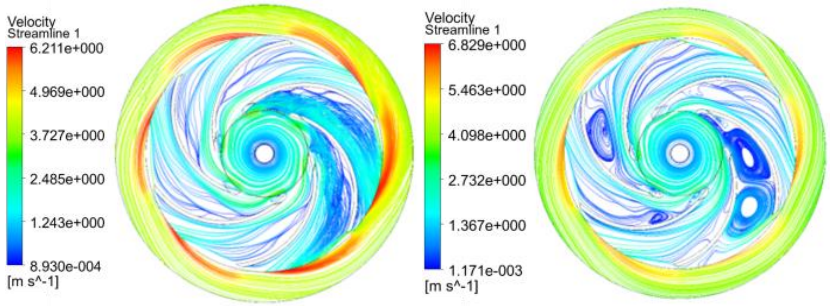

(a) Q=0.5Qd (b) Q=0.4Qd

Fig. 9 Control effect of groove width 0.5mm on stall vortex at Q=0.5Qd and Q=0.4Qd conditions

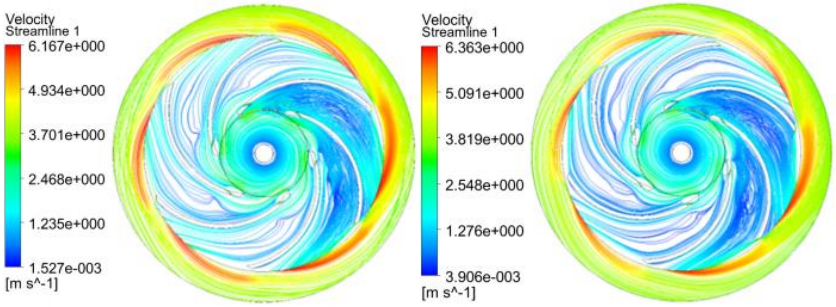

(a) Q=0.5Qd (b) Q=0.4Qd

Fig. 10 Control effect of groove width 1mm on stall vortex at Q=0.5Qd and Q=0.4Qd conditions

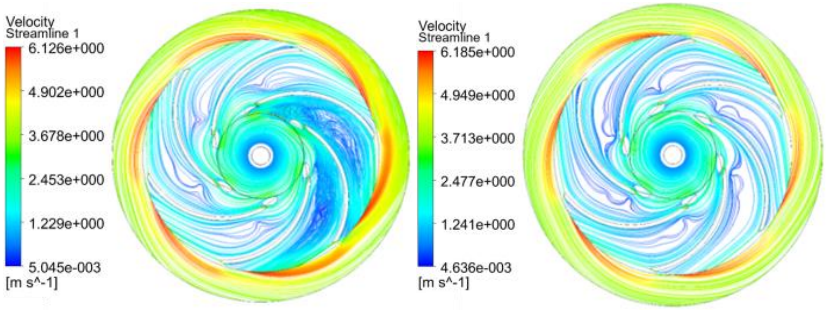

(a) Q=0.5Qd (b) Q=0.4Qd

Fig. 11 Control effect of groove width 2mm on stall vortex at Q=0.5Qd and Q=0.4Qd conditions

as depicted in Fig.8 to Fig. 12. Firstly, for the impeller with groove width of 0.25mm, the flow field characteristics filled with vortex structure under different flow conditions were presented. This indicates that when the groove width was too small, it became challenging to provide sufficient energy to suppress the fusion of the vortex structure near the channel inlet and the impeller shroud. With the increase in groove width, the vortex structure in the impeller is significantly restrained under Q=0.5Qd condition, as shown in Fig. 9 (a). However, the vortex structure still persisted in the impeller channel under Q=0.4Qd condition. When the groove width was set to 1mm, the stall vortex in the impeller was effectively restrained, even when the flow rate is reduced to Q=0.4Qd, as shown in Fig. 10 (b). However, as the groove width continued to increase as shown in Figs.11 and 12, although the vortex size in the impeller was noticeably restrained, the excessive groove width lead to

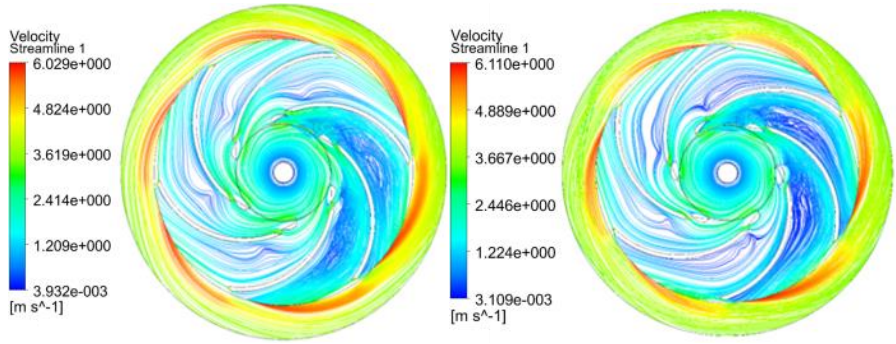

(a) Q=0.5Qd (b) Q=0.4Qd

Fig. 12 Control effect of groove width 3mm on stall vortex at Q=0.5Qd and Q=0.4Qd conditions

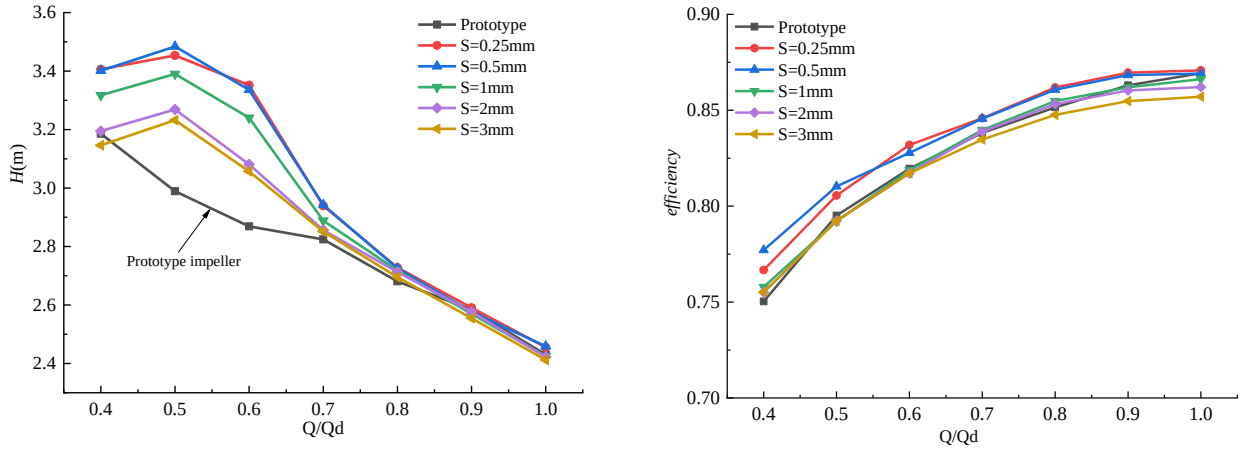

(a) impeller head (b) impeller efficiency

Fig. 13 External characteristics of impellers with different groove widths

more flow being sucked from the blade pressure side to the suction side of the subsequent channel. Therefore, the flow streamline was distorted near the groove position at the pressure side, particularly near the flow rate condition Q=0.4Qd.

A comparison between Fig. 8 and Fig. 12 reveals that when the groove width was greater than 1mm, the jet flow basically inhibited the stall vortex. To further determine the reasonable groove width, the influence of different groove width on impeller head and efficiency was further investigated, as shown in Fig.13. Firstly, for the impeller head curve, when the flow rate was greater than Q=0.7Qd, the head of prototype impeller was basically the same as that of the grooved impellers. This is mainly because the flow field in the impeller prototype remains relatively smooth under these conditions, and the grooved impeller dose not play significant role at those conditions. As shown in Fig. 4(c), tiny vortex structures alternated on the blade suction side at the condition Q=0.68Qd. The impeller head also begins to show a small difference, indicating that the grooved impellers started to suppress the vortex structure. When the flow rate was less than Q=0.68Qd, the head of groove impeller has been significantly improved. The impeller head with clearance of 0.25mm and 0.5mm was basically the same. With the increase of groove width, the impeller head showed a certain downward trend. When the groove width was greater than 2mm, the decreasing trend of impeller head remained consistent. However, it is intriguing that the impeller head increased most significantly at such a small groove width (d=0.25mm), as seen at Q=0.5Qd. As shown in Fig.8 (a), although there was a vortex structure in each impeller channel, the overall flow field in the impeller was more uniform compared with the impeller prototype. In addition, due to the existence of stall vortex, the blade suction side of each impeller channel was basically covered by stall vortex, while the flow on the pressure side was relatively smooth. The existence of grooves altered the distribution characteristics of flow field in the impeller.

For the impeller efficiency, the efficiency of the impeller with a groove width of 1mm is consistent with that of the prototype impeller. As the groove width increases, the efficiency of groove impeller decreased significantly near the design flow rate condition. With the decrease of flow rate, the efficiency of the impellers with different groove width was basically the same. When the groove size was less than 0.5mm, its efficiency was consistent with that of the prototype impeller near the design condition. With the decrease in flow rate, their efficiency was significantly higher than that of other impeller forms. The efficiency of the two grooved impellers with a gap of 0.5mm and 0.25mm was basically the same.

From Fig. 13, it can be seen that when the groove width was less than 0.5mm, although the control effect on stall vortex was not the best, the head and efficiency have been significantly improved for such a small groove

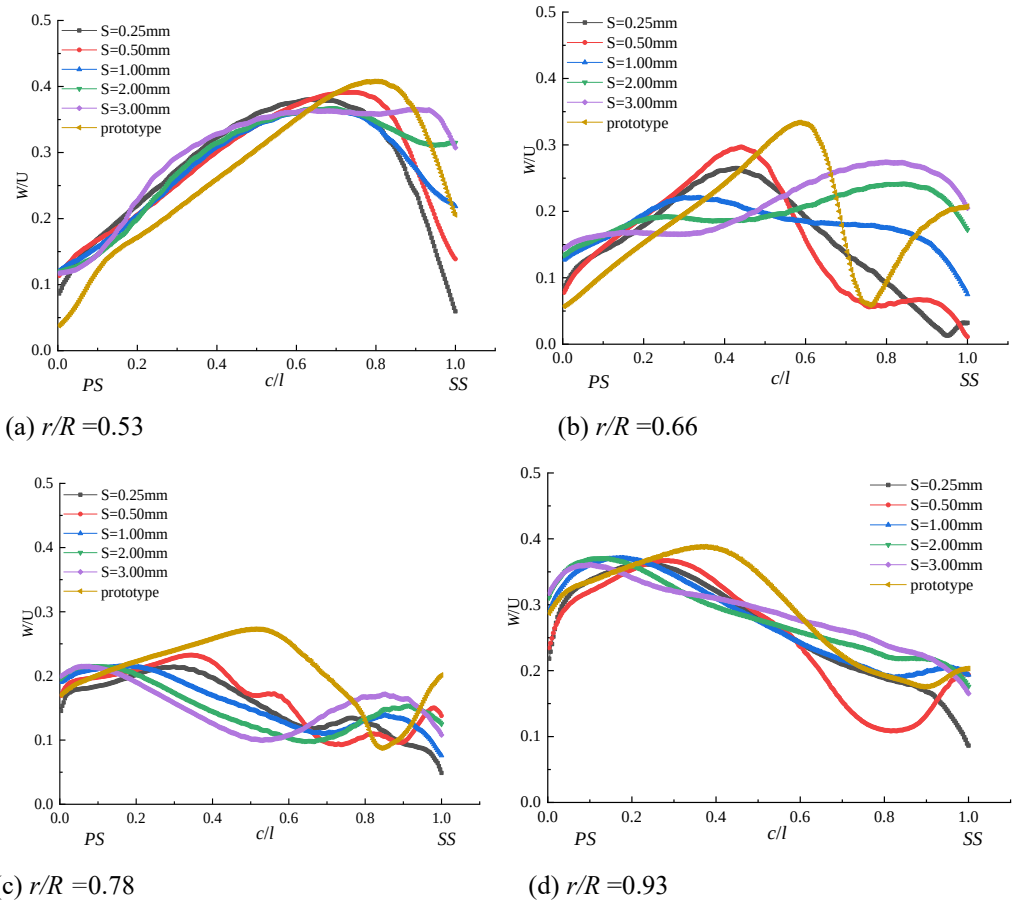

(a) *r/R* =0.53 (b) *r/R* =0.66

(c) *r/R* =0.78 (d) *r/R* =0.93

Fig. 14 Velocity distribution on different sample lines of non-stall flow channel under Q=0.7Qd condition

size. Next, the main reasons for this phenomenon were further analyzed. In fact, there is a direct relationship between the improvement of impeller performance and the velocity distribution in the impeller channels. In order to further explain the reasons for the obvious improvement of impeller head and efficiency when the groove width was less than 0.5mm, the velocity distribution of different impeller forms near the stall initial conditions was analyzed. Specifically, four circular arc sample lines centered on the impeller were selected at different radial relative positions in the impeller channel, with the radius ratios of *r*/R=0.53, *r*/R=0.66, *r*/R=0.78 and *r*/R=0.97, respectively. The sample line started at the blade pressure side and ends at the blade suction side. From the external characteristics of the impeller, it indicated that when the flow rate was less than Q=0.7Qd, the head of the prototype impeller and the grooved impeller began to show obvious differences. Therefore, the velocity distribution of different sample line positions in adjacent channels at Q=0.6Qd and Q=0.7Qd conditions was compared. The Fig.14 shows the velocity distribution on sample lines at Q=0.7Qd condition, where *W* represents the relative velocity and *U* represents the blade velocity at the impeller outlet.

For the non-stall channel, the velocity distribution trend, where the velocity was higher near the suction side and lower near the pressure side at *r/R* =0.53. The velocity near the blade pressure side of the prototype impeller was lower, while it was higher near the suction side. At *r/R* =0.66, the velocity near the pressure side of the prototype impeller was still lower than that of other impeller forms, and there was a high velocity area near the middle of the flow channel. At the outlet of the flow channel (*r/R* =0.78 and *r/R* =0.93), the velocity of different impeller forms was similar on both the pressure and suction sides. In the middle of the channel, the velocity of the prototype impeller was higher than that of the grooved impellers. Based on velocity distribution in the non-stall channel, the velocity near the pressure side of the grooved impeller was significantly higher, while the velocity in the middle of the channel was lower, compared with the prototype impeller.

In the stall channel as shown in Fig.15, the velocity of the prototype impeller was lower near the blade area, while the velocity in the middle of the flow channel was higher compared with grooved impeller from *r/R* =0.53 to *r/R* =0.78. At the impeller outlet in Fig.15 (d), the grooved impeller has higher velocity near the blade area compared to the impeller prototype. Therefore, combined with the velocity distribution in the adjacent two impeller channels, it is shown that the overall velocity distribution of the grooved impeller was more uniform. The velocity near the blade area increased significantly, especially near the blade pressure side.

As shown in Fig. 13 (a), the head of the grooved impeller was slightly improved compared with that of the prototype impeller at the flow rate of Q=0.7Qd. There was a significant difference in the head of impeller at the

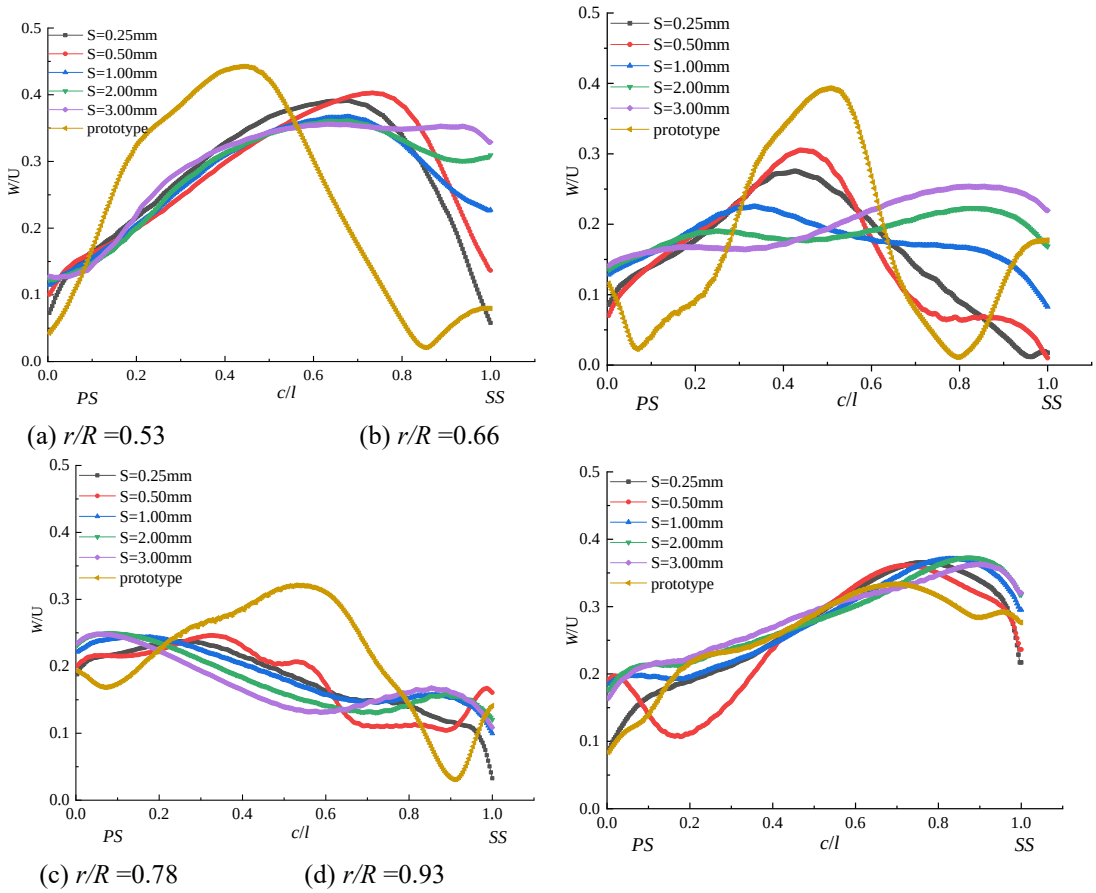

Fig. 15 Velocity distribution on different sample lines of stall channel under Q=0.7Qd condition

condition of Q=0.6Qd. To further verify that that the increase of the impeller head was attributable to the higher velocity in the vicinity of the blade pressure side. Fig. 16 presents the velocity distribution in two adjacent impeller channels under Q=0.6Qd condition. For non-stall channel, the velocity value of grooved impeller in the proximity of the pressure side was notably higher, while the velocity value in the vicinity of the suction side was lower than that of the original impeller model for the location r/R<0.66. When the groove width was less than 0.5mm, the velocity value on the blade suction side is lower than that of the impeller with a groove width greater than 0.5 mm. At the impeller outlet r/R>0.78, the velocity of the prototype impeller was higher.

For the stall channel in Fig. 16, when a stall vortex occurs in the impeller, the velocity near both the blade suction and pressure side decreased significantly but increase significantly in the middle position of the channel for the prototype impeller. The velocity in the grooved impeller exhibited the opposite trend. Therefore, the primary reason for the increase in impeller head was that the grooved impellers alter the velocity distribution characteristics in the stall channel, resulting in higher velocity near the blade area, particularly near the blade pressure side. The blade pressure side serves as the "work surface" of the impeller, which results in that the grooved impeller has a higher head.

Next, the velocity characteristics in the groove were analyzed. Taking the groove size of 1mm as an example, an axial sample line for velocity in the groove was set from the impeller shroud to hub. As shown in Fig. 17, the characteristics of velocity distribution in the groove at different flow rate conditions are presented. As shown in Fig. 17 (a), under Q=1.0Qd condition, the velocity on the sample line basically decreases slowly from the hub to shroud. When the flow rate decreased from Q=1.0Qd to Q=0.7Qd, a low-velocity region appears in the middle of the sample line. In fact, the velocity distribution characteristics in the gap can reflect the change of velocity distribution in the impeller channel during flow rate reduction process. Before stall vortex occurs, as the flow rate decreased from Q=1.0Qd to Q=0.7Qd, the velocity near the impeller shroud and hub remains relatively stable. While the velocity in the middle position of the flow channel tended to decrease rapidly. When stall vortex emerged, the velocity distribution trend on the sample line coincided with that under the design condition, indicating that the flow field within in the impeller returned to a more stable state.

Based on velocity distribution on sample line, as shown in Fig. 17(b), the average velocity in groove first decreased and then increased. This illustrates that when there was no stall vortex in the impeller, the velocity in the groove decreased as the flow rate decreases. However, when stall vortex emerged in the impeller, the velocity in groove increased with the decrease of flow rate. When the stall vortex developed more seriously, the jet flow velocity was higher in the groove. Therefore, the jet flow can play a dynamic regulatory role based on the

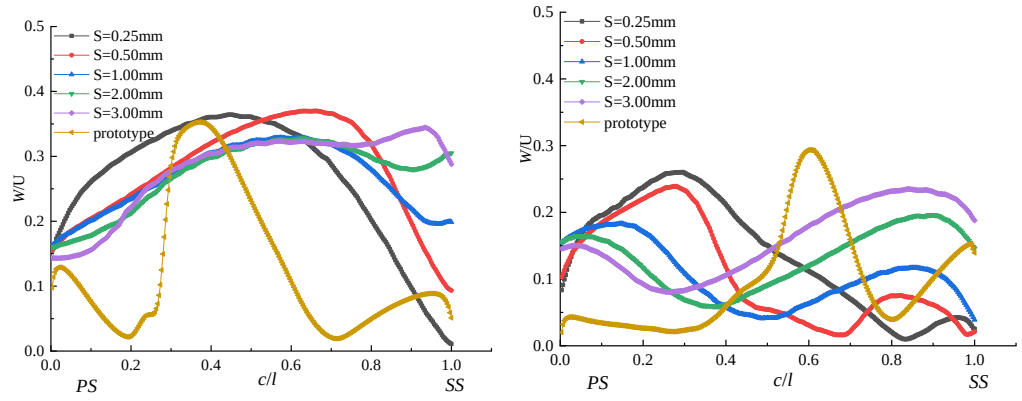

(a) *r*/*R* =0.53 (b) *r*/*R* =0.66

(c) *r*/R =0.78 (d) *r*/R =0.93

Fig. 16 Velocity distribution on different sample lines of stall flow channel at Q=0.6Qd condition

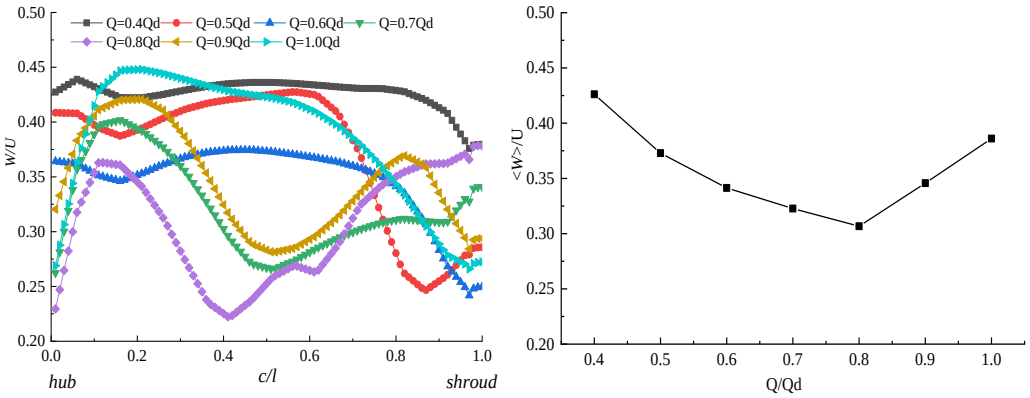

(a) axial velocity distribution (b) average velocity distribution

Fig. 17 Characteristics of velocity distribution in groove at different flow rate condition

flow field characteristics in the impeller.

The above research demonstrates that the grooved impeller can significantly enhance the impeller head at part-load flow conditions by changing the velocity distribution in channels. Subsequently, the impact of the groove on the flow field stability was further analyzed. The Fig. 18 presents a comparison of time-averaged results of groove and prototype impeller at Q=0.6Qd condition. The steady calculation results were relatively similar to the time-averaged results for the impeller utilized in this paper. The grooved impeller evidently inhibited the occurrence of alternating stall and the flow field in each impeller channel was relatively smooth, which further indicated that the grooved impeller exhibited superior performance.

Next, a further comparison was made on the characteristics of pressure pulsation for grooved and prototype impellers. As shown in Fig. 18 (a), two pairs of sample points in adjacent flow channels were selected. Sample points 1 and 2 are located near the blade suction

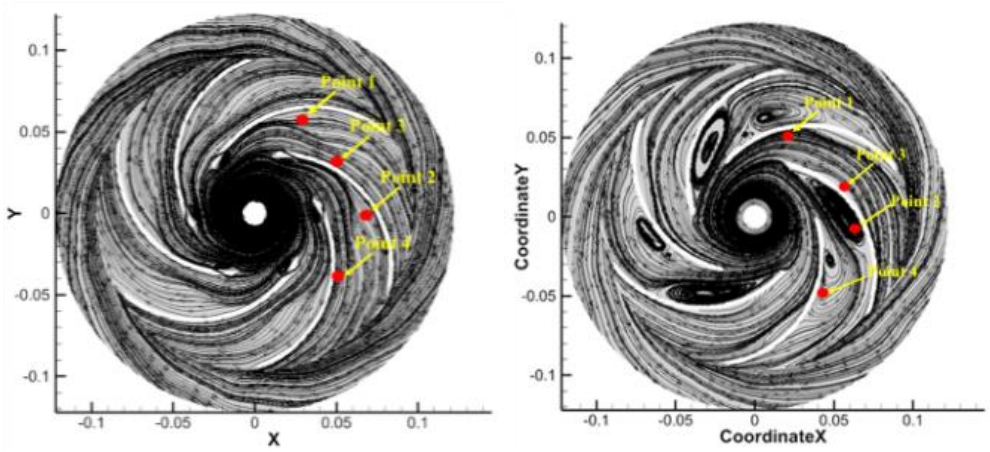

(a) grooved impeller (b) prototype impeller

Fig. 18 Time-average velocity comparison between grooved impeller and prototype impeller at Q=0.6Qd condition

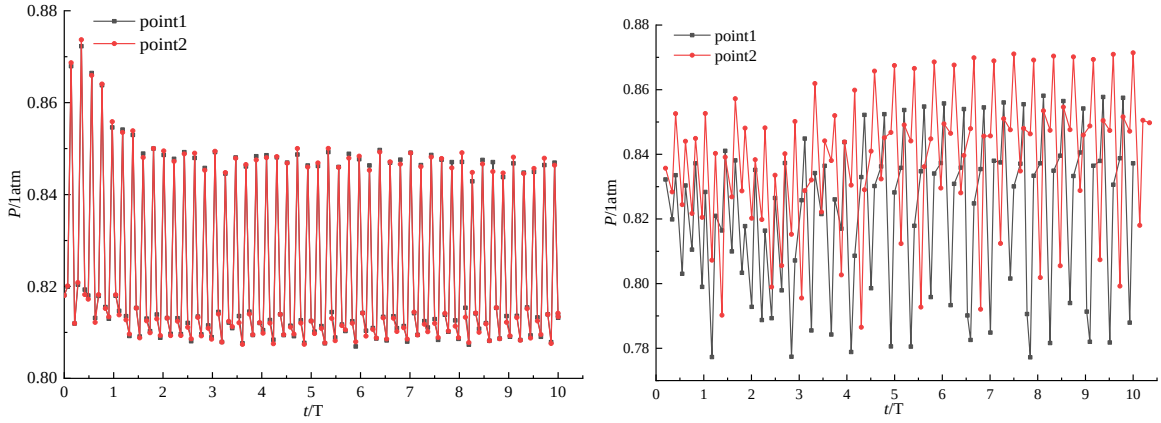

(a) grooved impeller (b) prototype impeller

Fig. 19 Comparison of pressure pulsation near the blade suction side between grooved and prototype impeller

side, while sample points 3 and 4 are near the blade pressure side. The positions of sample points in the grooved impeller are consistent with that of prototype impeller. As illustrated in Fig. 19(a) for the grooved impeller, the pressure pulsation characteristics near the blade suction side in two adjacent channels were basically the same. This also indicated that the flow in grooved impeller channels was more uniform. Therefore, for the grooved impeller, both the time-averaged flow field and the instantaneous flow field structure remained consistent in each impeller channel. However, as shown in Fig. 19(b) for the prototype impeller, there were distinct differences in the instantaneous pressure pulsations in the adjacent impeller channels.

Figure 20(b) compares the pressure pulsation near the blade pressure side of adjacent channels for grooved and prototype impellers. For two different sample points near the pressure side, the instantaneous flow field in the impeller remained basically stable after four impeller cycles. Whether for stall channel or non-stall channel, the pressure pulsation in the grooved impeller decreases was significantly reduced. By comparing the instantaneous pressure fluctuation at different sample points near the blade pressure side, it was revealed that the pressure fluctuation value in grooved impeller was significantly lower than that of the prototype impeller. This further indicates that the stall vortex typically introduced additional pressure pulsation, while the grooved impeller could enhance the stability of the internal flow characteristics within the impeller.

4. DISCUSSION

Despite the numerous methods available for controlling the stall in the impeller, the mechanism of stall and the formation process of stall vortex remain unclear. Most scholars believe that stall is closely related to the inlet angle at the channel inlet. As a result, the focus is laid on modifying the blade leading edge. Additionally, by adding short blades in the impeller channel, the external characteristics of the impeller can be significantly changed. While these methods can to some extent weaken stall, but they do not fundamentally inhibit stall. Moreover, these modifications may potentially

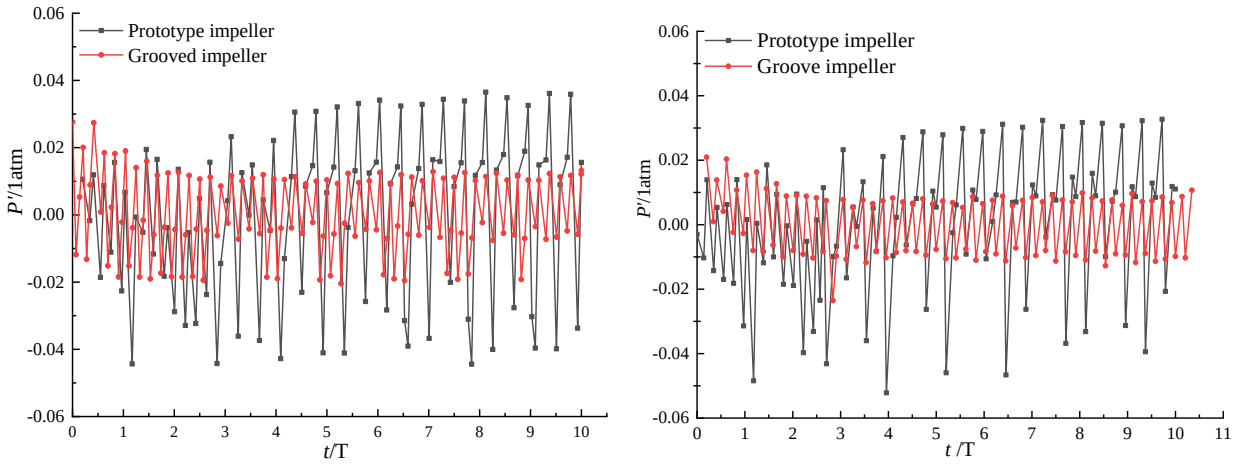

(a) sample point 3 (b) sample point 4

Fig. 20 Pressure pulsation near the blade pressure side for grooved and prototype impellers

modify the external performance of the impeller under the design flow rate condition. Based on the stall mechanism, the grooved impeller inhibits the formation of vortex structure by blocking the fusion of vortices at two different positions in the impeller, resulting in a more stable flow field. Meanwhile, it can also significantly delay the stall inception and also ensure that external performance of the impeller near the design flow conditions remains unchanged. Therefore, setting a groove at the appropriate position of the blade inlet is an effective method for controlling the stall vortex and stabilizing the internal flow field within the impeller.

5. CONCLUSION

Based on the stall mechanism in the impeller, this paper proposed an effective control method for stall and conducted a thorough analysis of the method's details and control mechanism. This stall control method could not only effectively suppress the stall vortex under part-load flow rate conditions, but also improve the impeller head. Moreover, it can ensure that the impeller external characteristics remain unchanged under the design condition. The main conclusions are as follows.

(1) The jet flow near the blade leading edge can effectively block the merging of the separation vortex at the impeller channel inlet and the twisted vortex strip near the impeller shroud, thereby inhibiting the generation of stall vortex. When a groove is formed near the blade inlet, the high-velocity jet blocks the increasing separation vortex at the channel inlet. Meanwhile, under the action of high-velocity jet flow, the twisted vortex strip near impeller shroud cannot induce flow separation near the middle position of the blade suction side, further inhibiting the emergence of vortex structure. Therefore, the groove method can control inception of the stall vortex at the source.

(2) The rational groove pattern holds great significance for the control effect of stall vortex. The optimal groove width is approximately 1mm. When the groove size is too large, the impeller head and efficiency are significantly reduced. Conversely, if the groove size is too small, the stall vortex suppression effect will be significantly weakened. Meanwhile, the optimal relative position of the groove is between *r*/R= 0.4 and 0.5. If the groove position is outside this relative range, it becomes challenging for the jet flow to prevent the separation vortex at the channel inlet from merging with the twisted vortex strip near the impeller shroud.

(3) The grooved impeller significantly enhances the impeller head, as it notably increases the velocity near the blade pressure side under part-load flow conditions. Nevertheless, the impact of grooves on efficiency improvement is relatively insignificant. Through comparing the velocity distribution in the impeller channels, it is revealed that velocity near the blade area escalates considerably, particularly near the blade pressure side. The pressure side serves as the “work surface” of the impeller, consequently resulting in a notable increase in the impeller head. Simultaneously, the disappearance of vortex structure and smoother flow within the grooved impeller constitute the primary reason for the enhancement of the impeller head.

(4) The grooved method can stabilize the flow in the impeller by suppressing the appearance of vortex structure. By comparing the pressure pulsations at different positions in the impeller under part-load flow rate conditions, the results show that the grooved impeller can ensure a more uniform flow field in the impeller. Meanwhile, the pressure pulsation in the impeller is significantly reduced by restraining the vortex structure. Therefore, the grooved impeller can significantly delay the stall inception and widen the stable operation range of the impeller.

ACKNOWLEDGMENTS

The study was financially supported by the National Natural Science Foundation of China (Grant No. 52179093, Grant No. 52379085, Grant No. 52276041).

CONFLICT OF INTEREST

The authors declare that they have no known competing financial interests or personal relationships

that could have appeared to influence the work reported in this paper

AUTHORS CONTRIBUTION

Xiao-Dong Liu: Write original draft, Methodology. **Xian-bei Huang:** Review and editing. **Yao-Jun Li:** Project administration. **Zhu-Qing Liu:** Funding acquisition, Investigation, Data curation. **Wei Yang:** Supervision.

REFERENCE

Adu, D., Du, J. G., Darko, R. O., Antwi, E. O., & Khan, M. A. S. (2021). Numerical and experimental characterization of splitter blade impact on pump as turbine performance. *Science Progress, 104*(2), 1-15. https://doi.org/10.1177/0036850421993247

Chiang, H. W. D., & Fleeter, S. (1991). *Flutter control of incompressible flow turbomachine blade rows by splitter blades.* 27th Joint Propulsion Conference. https://doi.org/10.1051/jp3:1994162

Cui, B. L., Zhang, C. L., Zhang, Y. L., & Zhu, Z. C. (2020) Influence of cutting angle of blade trailing edge on unsteady flow in a centrifugal pump under off-design conditions. *Applied Sciences, 10*(2), 1-16. https://doi.org/10.3390/app10020580

Cui, B., Zhu, K., Zhang, Y., & Lin, P. (2019). Experimental and numerical study of the performance and cavitation flow of centrifugal pump with jetting device. *Journal of Mechanical Science and Technology, 33*(10), 4843-4853. https://doi.org/10.1007/s12206-019-0925-6

Davood, K., & Shirani, E. (2018). Influences of impeller splitter blades on the performance of a centrifugal pump with viscous fluids. *International Journal of Fluid Machinery and Systems, 11*(4), 400-411. https://doi.org/10.5293/ IJFMS.2018. 11.4. 400

Du, Q. A., Zhu, J. Q., Zhou, M., & Li, W. (2011). Computational investigation of blade slotting on a high-load low-pressure turbine profile at various reynolds numbers: Part I-Slotting scheme's verification. *Journal of Thermal Science, 20*(1), 13-20. https://doi.org/10.1007/s11630-011-0428-y

Gölcü, M., & Pancar, Y. (2005). Investigation of performance characteristics in a pump impeller with low blade discharge angle. *World Pumps, 0*(468), 32–40. https://doi.org/10.1016/S0262-1762 (05)70749-5

Gölcü, P. Y., & Sekmen, Y. (2006). Energy saving in a deep well pump with splitter blade. *Energy Conversion and Management, 47*(5), 638–651. https://doi.org/10.1016/j.enconman.2005.05.001

Guo, S. J., & Maruta, Y. (2005). Experimental investigations on pressure fluctuations and vibration of the impeller in a centrifugal pump with vaned diffusers. *JSME International Journal Series B Fluids and Thermal Engineering, 48*(1), 136-143. https://doi.org/10.1299/jsmeb.48.136

Jadidi, M., Bazdidi-Tehrani, F., & Kiamansouri, M. (2018). Scale-adaptive simulation of unsteady flow and dispersion around a model building: spectral and POD analyses. *Journal of Building Performance Simulation, 11*(2), 241-260. https://doi.org/10.1108 /EC-04-2019-0147

Jia, X. Q., Yuan, S., Zhu, Z. C., & Cui, B. L. (2019). Numerical study on instantaneous radial force of a centrifugal pump for different working conditions. *Engineering Computations. 37*(2), 458-480. https://doi.org/ 10.1108/EC-04-2019 -0147

Kergourlay, G., Younsi, M., Bakir, F., & Rey, R. (2007). Influence of splitter blades on the flow field of a centrifugal pump: test-analysis comparison. *International Journal of Rotating Machinery*, *2007*. https://doi.org/10.1155/2007/85024

Khoeini, D., & Shirani, E. (2019). Influences of diffuser vanes parameters and impeller micro grooves depth on the vertically suspended centrifugal pump performance. *Journal of Mechanics. 35*(5), 735-746. https://doi.org/10.1017/jmech. 2019. 13

Korkmaz, G, M., & Kurbanoğlu, C. (2017). Effects of blade discharge angle, blade number and splitter blade length on deep well pump performance. *Journal of Applied Fluid Mechanics, 10*(2), 529-540. https://doi.org/10.18869/acadpub.jafm.73.238.26056

Liu, X. D., Farhat, M., Li, Y. J., Liu, Z. Q., & Yang, W. (2023). Onset of flow separation phenomenon in a low-specific speed centrifugal pump impeller. *Journal of Fluids Engineering, 145*(2), 021206. https://doi.org/10.1115/1. 40562 13

Liu, X. D., Li, Y. J., Liu, Z. Q., & Yang, W. (2022). Dynamic stall inception and evolution process measured by high-frequency particle image velocimetry system in low specific speed impeller. *Journal of Fluids Engineering*, *144*(4), 041504. https://doi.org/10.1115/1.4053166

Lu, J. X., Zeng, Y. Z., Zhu, B. S., Hu, Bo., & Hua, H. (2020). Investigation of the noise induced by unstable flow in a centrifugal pump. *Energies, 13*(3), 589. https://doi.org/10.3390/en13030589

Luo, H. Y, Tao, R., Yang, J. D., & Wang, Z. W. (2020). Influence of blade leading-edge shape on rotating-stalled flow characteristics in a centrifugal pump impeller. *Applied Sciences, 10*(5635), 5635. https://doi.org/10.3390/app10 16563 5

Onoue, O, A., Hayakawa, M., & Kawata, Y. (2016). Study on improvement of suction performance for industrial pumps by applying splitter blade. *Turbomachinery, 44*(2), 73–80. https://doi.org/10.1177/09544062211027608

Pedersen, N., Larsen, P. S., & Jacobsen, C. B. (2003). Flow in a centrifugal pump impeller at design and off-design conditions—Part I: Particle image

velocimetry (PIV) and laser doppler velocimetry (LDV) *Measurements. Journal of Fluids Engineering, 125*(1), 61–72. https://doi.org/10.1115/1.1524585

Sato, F. A., & Takamatsu, Y. (1993). Influence of impeller blade angles of centrifugal pump on air/water two-phase flow performance. *Nihon Kikai Gakkai Ronbunshu, B Hen/Transactions of the Japan Society of Mechanical Engineers, Part B, 59*(567), 3513-3518. https://doi.org/10.1299/kikaib.59.3513

Shigemitsu, F. J., Kaji, K., & Wada, T. (2013). Unsteady internal flow conditions of mini-centrifugal pump with splitter blades. *Journal of Thermal Science, 22*(1), 86-91. https://doi.org/ 10.1007/ s11630-013-0596-z

Shojaeefard, T, M., Ehghaghi, M., Fallahian, M., & Beglari, M. (2012). Numerical study of the effects of some geometric characteristics of a centrifugal pump impeller that pumps a viscous fluid. *Computers & Fluids*, 61-70. https://doi.org/10.1016/j.compfluid. 2012.02.028

Song, P. F., Zhang, Y. X., Xu, C., Zhou, X., & Zhang, J. Y. (2015). Numerical studies on cavitation behavior in impeller of centrifugal pump with different blade profiles. *IJFMS, 8*(2), 94-101. https://doi.org/10.5293/IJFMS. 2015.8.2.094

Kyparissis, S. D., & Margaris, D. P. (2012). Experimental investigation and passive flow control of a cavitating centrifugal pump. *International Journal of Rotating Machinery,* 1–8. https://doi.org/10.1155/2012/ 248082

Tanaka, H. (2011). Vibration behavior and dynamic stress of runners of very high head reversible pump-turbines. *International Journal of Fluid Machinery and Systems, 4*(2), 289-306. https://doi.org/ 10.5293/IJFMS.2011.4.2.289

Wu, X. F., Sun, X. L., Tan, M. G., & Liu, H. L. (2021). Research on operating characteristics of a centrifugal pump with broken impeller. *Advances in Mechanical Engineering, 13*(9). https://doi.org/10.1177/16878140211049951

Ye, W. X., Zhu, Z. C., Qian, Z. D., & Luo, X. W. (2020). Numerical analysis of unstable turbulent flows in a centrifugal pump impeller considering the curvature and rotation effect. *Journal of Mechanical Science and Technology, 34*(7), 2869-2881. https://doi.org/10.1007/s 12206-020-0619-0

Yuan, Y., & Yuan, S. Q. (2017). Analyzing the effects of splitter blade on the performance characteristics for a high-speed centrifugal pump. *Advances in Mechanical Engineering, 9*(12). https://doi.org/10.1177/ 1687814017745251

Zhao, X. R., Xiao, Y. X., Wang, Z. W., Luo, Y. Y., & Cao, L. (2018). Unsteady flow and pressure pulsation characteristics analysis of rotating stall in centrifugal pumps under off-design conditions. *Journal of Fluids Engineering. 140*(2), 021105. https://doi.org/10.1115/1.4037973

Zhou, X. Y., Zhao, Q. J., Cui, W. W., & Xu, J. Z. (2017). Investigation on axial effect of slot casing treatment in a transonic compressor. *Applied Thermal Engineering, 126*(1), 53-69. https://doi.org/10.1016/j.applthermaleng.2017.07.165

Zhu, J., Chu, W., & Lu, X. (2006). Design and experimental investigations of a new type of casing treatment for an axial flow compressor. *Proceedings of the Institution of Mechanical Engineers, Part A: Journal of Power and Energy, 220*(3), 207-215. https://doi.org/10.1243/09576509JPE139